OFFSET-CONTINUATION STACKING

T.A. Coimbra, A. Novais, and J. Schleicher

email: *tgo.coimbra@gmail.com,amelia@ime.unicamp.br,js@ime.unicamp.br*
keywords: *Offset continuation, data stacking, signal enhancement, multi-fold data*

ABSTRACT

We introduce a data-driven stacking technique that transforms 2D/2.5D prestack multicoverage data into a common-offset (CO) section. We refer to this new process, which is based on the offset-continuation operation (OCO), as offset-continuation stacking or briefly OCO stack. Similarly to the CMP and CRS stacks, the OCO stack does not rely on an a-priori velocity model but provides velocity information itself. The original OCO method is a seismic configuration transform designed to simulate a seismic section as if obtained with a certain source-receiver offset using the data measured with another offset. Since OCO is dependent on the velocity model used in the process, it can be combined with stacking techniques for a set of models, thus allowing for the extraction of velocity information. The algorithm is based on so-called OCO trajectories, which are related to the concepts of image waves and velocity rays. We theoretically relate the OCO trajectories to the kinematic properties of OCO image waves that describe the continuous transformation of the common-offset reflection event from one offset to another. Based on OCO trajectories, we then formulate a horizon-based velocity analysis method, where root mean square (RMS) velocities and local event slopes are determined by stacking along event horizons.

INTRODUCTION

By definition, the Offset-Continuation Operation (OCO) is an operator that transforms common offset (CO) seismic gathers from one constant offset to another (Deregowski and Rocca, 1981). It is an important tool for imaging in a complex medium. Possible applications of OCO include velocity analysis, common-reflection point (CRP) stacking, dip moveout (DMO), migration to zero offset (MZO), interpolation of missing data, amplitude variation with offset (AVO) studies, and geometrical-spreading correction (see, e.g., Salvador and Savelli, 1982; Bolondi et al., 1982, 1984; Fomel, 1994, 2003; Santos et al., 1997).

Since OCO is a configuration transform, its objective is to simulate a seismic section using as input the data measured with another configuration. As discussed by Hubral et al. (1996a) and mathematically demonstranted by Tygel et al. (1996), any configuration transform can be thought of as being composed of a migration and a subsequent demigration after changing a configuration parameter.

Configurations transforms have already been used for several purposes in seismic processing such as MZO (Tygel et al., 1998; Bleistein et al., 1999), source continuation operation (SCO) (Bagaini and Spagnolini, 1993, 1996), azimuth moveout (AMO) (Biondi et al., 1998), DMO (Hale, 1984; Canning and Gardner, 1996; Collins, 1997; Black et al., 1993), common-source (CS)-DMO (Schleicher and Bagaini, 2004), data reconstruction (Bagaini et al., 1994; Stolt, 2002; Chemingui and Biondi, 2002), and velocity analysis (Silva, 2005; Coimbra et al., 2012).

For data of very low signal-to-noise ratio (S/N) or acquisitions with very low fold, conventional common-midpoint (CMP) processing might not provide stacked sections of sufficient quality. In such situations, alternative processing sequences are necessary to improve the data quality. The OCO stack represents such an alternative path for the processing of reflection-seismic data. Its key element is the construction of common-offset stacked sections together with coherency sections and sections of kinematic

and dynamic wavefield attributes.

The OCO stacking surface is composed of so-called OCO trajectories (Coimbra et al., 2012). Such a trajectory requires only two parameters (local event slope and stacking velocity) to describe the seismic reflection event in the multi-coverage data. Neighbouring trajectories can be located by event tracking in the stacked section or described by a third curvature-related parameter. Using these parameters, the method stacks the data along a predicted traveltime curve that approximates the CRP event. Since the parameters, and thus the predicted traveltime curve, are updated from the data at each offset, the approximation is better than by conventional methods that adjust the approximate traveltime expression at some initial point. The purpose of this paper is to establish a consistent processing chain that is based entirely on the OCO stack, relying on identical assumptions at all steps.

METHOD

The OCO stack is a multiparameter stacking procedure similar to its relatives, the CMP and CRS stacks and multifocusing. It automatically determines stacking attributes based on a coherence measure applied at every common-offset sample of the data. Since these attributes vary with time for the same event, the OCO stacked section is free of normal moveout (NMO)-stretch (Perroud and Tygel, 2004). The main advantages of the OCO stack are twofold. Firstly, it is not limited to a zero-offset stacked section like the CMP stack. Secondly, for the 2D/2.5D case as discussed here, the OCO stack needs at most two parameter in addition to stacking velocity, even for the construction of stacked common-offset sections.

There are other multiparameter stacking methods (Gelchinsky et al., 1999; Jäger et al., 2001; Zhang et al., 2001; Hertweck et al., 2007; Fomel and Kazinnik, 2012), which are based on stacks data from multiple CMP locations. As a result, they considerably improve the signal-to-noise ratio. However, these methods require the estimation of more data parameters than conventional CMP processing, in addition to the conventional stacking velocity. For instance, the zero-offset CRS method requires two additional parameters and common-offset CRS requires four of them. Moreover, due to multi-coverage some events such as diffractions, far-offset faults and strong dips can disappear.

In this section, we derive the theoretical basis for the OCO stack. It is based on the kinematic behaviour of the OCO transformation as described by the OCO image-wave equation (Hubral et al., 1996b).

Image-wave for OCO

The OCO image-wave equation was derived through image-wave theory from the kinematic behaviour of the OCO transformation (Hubral et al., 1996b). It is a second order linear partial differential equation, which can be written as

$$ht\left(\frac{\partial^2 U}{\partial h^2}+\frac{4}{V^2}\frac{\partial^2 U}{\partial t^2}\right)+\left(t^2+\frac{4h^2}{V^2}\right)\frac{\partial^2 U}{\partial h\partial t}-ht\frac{\partial^2 U}{\partial \xi^2}=\Theta\left(\xi,t,h,U,\frac{\partial U}{\partial \xi},\frac{\partial U}{\partial t},\frac{\partial U}{\partial h}\right). \quad (1)$$

Equation (1) describes the behavior of an *artificial* (non-physical) process of transforming reflection seismic data $U(\xi,t,h)$ in the offset-midpoint-time domain as a certain kind of "wave propagation". In this case it is the record of the seismic reflection that "propagates"as a function of half-offset h. In equation (1), ξ and t are the midpoint and time coordinate of the reflection event under consideration. The velocity V is assumed to be a constant average velocity that is known a priori. We will refer to V as the OCO velocity. Its relationship to the RMS velocity is discussed below.

Equation (1) belongs to the class of linear hyperbolic equations, when $t>0$ and $h\neq 0$, with the half-offset h acting as propagation variable (i.e., equivalent to time in conventional wave propagation). Equation (1) describes a wave-like propagation in the offset direction that Hubral et al. (1996b) termed image-wave propagation.

We use the OCO image-wave equation (1) to obtain the trajectory of single point under variation of the half-offset. Formally, we can think of the solution to equation (1) as being approximated by an expression that is analogous to the one used in ray theory, i.e., the leading term of a high-frequency asymptotic (WKBJ-type) approximation for a reflected wave recorded on a seismogram of the form

$$U(\xi,t,h)=A(\xi,t)F(h-H(\xi,t)), \quad (2)$$

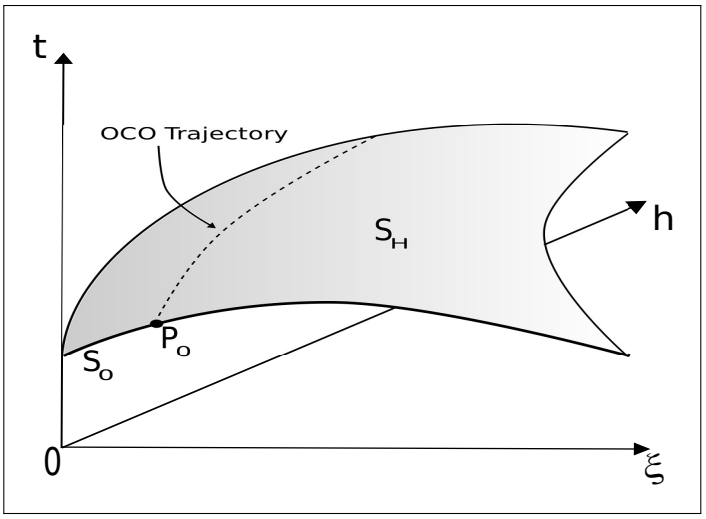

Figure 1: *Sketch representing a traveltime surface and an OCO trajectory starting at a point P_0 on the traveltime curve S_0 in the initial common-offset section with half-offset h_0 (front panel).*

where A stands for the amplitude, F is the wavelet shape of the leading high-frequency term, and $H = H(\xi, t)$ describes the image-wave front for the OCO image wave. In other words, H can be called the OCO eikonal. By substitution of approximation (2) in equation (1), we obtain, to the leading order, the image-eikonal equation associated with equation (1) as

$$tH\left(1+\frac{4}{V^2}\left(\frac{\partial H}{\partial t}\right)^2\right)-\left(t^2+\frac{4}{V^2}H^2\right)\frac{\partial H}{\partial t}-tH\left(\frac{\partial H}{\partial \xi}\right)^2=0. \tag{3}$$

Equation (3) kinematically describes the propagation of the OCO image-waves.

OCO Trajectories

The solution of the OCO eikonal equation (3) leads to ray-like trajectories describing the position of a selected point P_0 on a seismic reflection event S_0 in different common-offset sections, the so-called OCO trajectories (Coimbra et al., 2012, see also Figure 1). In this section, we develop an algebraic procedure to construct the OCO trajectories. It is based on manipulating the Huygens image-wave for OCO (Hubral et al., 1996b).

We begin our derivation with the Cauchy-problem consisting of the first-order differential equation (3) and initial condition

$$H(\xi_{h_0}, t_{h_0}(\xi_{h_0})) = h_0, \tag{4}$$

where h_0 denotes the initial half-offset, i.e., the one at which the OCO trajectory starts. Note that h_0 can be any offset, not only zero offset as in the CMP method or zero-offset CRS.

Coimbra et al. (2012) used the method of characteristics to obtain the analytical form for the OCO trajectories. This method consists of transforming equation (3) into the following system of ordinary dif-

ferential equations

$$\begin{aligned}
\frac{d\xi}{dh} &= -2\lambda tHp, \\
\frac{dt}{dh} &= -\lambda\left(4H^2 - 8qtH + t^2V^2\right)/V^2, \\
\frac{dp}{dh} &= -\lambda\left[tp\left(1-p^2\right) + 4pq\left(tq - 2H\right)/V^2\right], \\
\frac{dq}{dh} &= -\lambda\left[\left(4q^2/V^2 - 1\right)\left(tq - H\right) - p^2\left(tq + H\right)\right], \\
\frac{dH}{dh} &= \lambda\left(-tHp^2 + 4q^2tH/V^2 - tH\right) \equiv 1,
\end{aligned} \tag{5}$$

where $p = \partial H/\partial\xi$ and $q = \partial H/\partial t$. The choice $dH/dh \equiv 1$ in the last equation is required to guarantee $h = H(\xi, t)$ on the OCO image-wavefront, i.e., on the seismic reflection event in the CO section for h. This defines the scale factor as $\lambda = \left(-tHp^2 + 4q^2tH/V^2 - tH\right)^{-1}$.

System (5) is called the *characteristic system of differential equations* of equation (3). All variables involved are parameterized as $\xi = \xi(h)$, $t = t(h)$, $p = p(h)$, $q = q(h)$ and $H = H(h)$. The solutions $(\xi(h), t(h))$ of system (5) describe the *OCO trajectory* associated with an initial point P_0 in the CO section with half-offset h_0 (see Figure 1). In other words, $(\xi(h), t(h))$ are the coordinates where the image of P_0 will be found in any other CO section with half-offset h.

According to the general theory of partial differential equations of the first order (Courant and Hilbert, 1989), we obtain the general manifold of solutions to the partial differential equation (3) with the initial value (4) by the following procedure. The traveltime surface in the offset-midpoint-time space is a manifold $S_H(t, \xi, H) = 0$ (see again Figure 1). At $h = h_0$, the manifold coincides with the reflection event $S_0 = S_H(t(h_0), \xi(h_0), h_0) = 0$. This manifold can alternatively be described by the parameter $\xi_{h_0} = \xi(h_0)$, where

$$\left(\frac{\partial\xi}{\partial\xi_{h_0}}\right)^2 + \left(\frac{\partial t}{\partial\xi_{h_0}}\right)^2 \neq 0 \tag{6}$$

must be satisfied in order to guarantee the existence of the OCO trajectories. Hence, we define S_0 as the traveltime curve in a common-offset section as the manifold S_H projected on the $\xi \times t$-common-offset-plane with $h = h_0$ and rewrite H, t, ξ as functions of the parameter ξ_{h_0}.

We now seek an integral surface $H(\xi, t)$ which passes through S_0, that is, a solution to (3)) for which $H(\xi_{h_0} = H(\xi(\xi_{h_0}), t(\xi_{h_0})) = h_0$ holds identically for all ξ_{h_0}. The curve S_0 is called the *initial curve* of the problem, and $H(\xi_{h_0})$ is called the *initial data*.

This leads to a family of characteristic curves

$$t = t(\xi_{h_0}, h), \tag{7}$$
$$\xi = \xi(\xi_{h_0}, h), \tag{8}$$
$$H = H(\xi_{h_0}, h), \tag{9}$$

which depend on ξ_{h_0} and h as parameters. Fixing $h = h_0$ and varying ξ_{h_0} we obtain the curve S_0. On the other hand, fixing ξ_{h_0} and varying h, we obtain the OCO trajectories.

Complete solution

The initial value problem composed by equations (3) and (4) can be solved analytically. Actually, Santos et al. (1997) have demonstrated that for one fixed ξ_{h_0}, all possible OCO trajectories must satisfy

$$t^2 = t(\xi, h, \xi_{h_0}, t_{h_0}, h_0)^2 = \frac{4h^2}{V^2} + \frac{4h^2(t_{h_0}^2 - 4h_0^2/V^2)}{u(h, h_0, \xi, \xi_{h_0})^2}\,, \tag{10}$$

with

$$u(h, h_0, \xi, \xi_{h_0}) = \sqrt{(h + h_0)^2 - (\xi - \xi_{h_0})^2} + \sqrt{(h - h_0)^2 - (\xi - \xi_{h_0})^2}. \tag{11}$$

Equation (10) is also known as the OCO Huygens-image curve. In analogy to physical wave phenomena, equation (10) is the position of a (hypothetical) image wave 'excited' at an elementary point-source at a position P_0 with coordinates (ξ_{h_0}, t_{h_0}) (Hubral et al., 1996b). In other words, equation (10) represents a *complete integral* of the problem (3)-(4), depending on the parameters ξ, h, ξ_{h_0}, t_{h_0} and h_0, but independently of the actual position of the event through P_0.

The actual path of the OCO trajectory depends on the event slope at P_0. To describe this dependence, we parameterize $t_{h_0} = t_{h_0}(\xi_{h_0})$ and consider ξ_{h_0} as a function of ξ, h and h_0. The envelope of all OCO Huygens image-curves for all points on S_0 describes the manifold S_H at half-offset h. It is constructed by taking the derivative of t in equation (10) with respect to ξ_{h_0}. Under consideration of the identity

$$\frac{dt}{d\xi_{h_0}} = \frac{\partial t}{\partial \xi_{h_0}} + \frac{\partial t}{\partial t_{h_0}} \frac{dt_{h_0}}{d\xi_{h_0}} = 0 \,, \tag{12}$$

this yields after several algebraic transformations

$$(\xi - \xi_{h_0}) = \frac{2\Upsilon_{h_0}(h^2 - h_0^2)}{\sqrt{\Upsilon_{h_0}^2 \eta^2 + 2t_{n_0}^4 + 2\sqrt{t_{n_0}^8 + \Upsilon_{h_0}^2 t_{n_0}^4 \eta^2 + 16\Upsilon_{h_0}^4 h^2 h_0^2}}} \,, \tag{13}$$

where $t_{n_0} = \sqrt{t_{h_0}^2 - 4h_0^2/V^2}$ is the NMO corrected traveltime at the initial half-offset h_0, $\eta = 2\sqrt{h^2 + h_0^2}$, and $\Upsilon_{h_0} = t_{h_0}\phi_{h_0}$, with

$$\phi_{h_0} = \frac{dt_{h_0}}{d\xi_{h_0}} \tag{14}$$

denoting the dip of the reflection event S_0 at P_0.

Together, equations (10) and (13) constitute a parametric form of the manifold S_H. For a fixed ξ_{h_0} these equations thus describe the OCO trajectory from P_0 in the initial common-offset section at h_0 to any other common-offset at h. In other words, equations (10) and (13) represent the position of events that are reflected at the same point in depth (if the medium was exactly described by the OCO velocity V), i.e., the OCO trajectory belongs to a common-reflection point (CRP). Using the formulae above, we can trace an OCO trajectory starting at any point on an reflection event in any arbitrary common-offset section, just using the information about the average velocity and local event slope at that point. If the OCO trajectory starts or ends at zero offset, formulae (10) and (13) simplify considerably.

Migration to zero offset. For a migration to zero offset, we need the OCO trajectory to start at some initial half-offset $h_0 \neq 0$ and end at the final half-offset $h = 0$. This reduces the set of equations (10) and (13) to

$$t_0^2 = t(\xi_0, \xi_{h_0}, t_{h_0}, h_0)^2 = t_{n_0}^2 \left(1 - \frac{(\xi_0 - \xi_{h_0})^2}{h_0^2}\right) \,, \tag{15}$$

$$\xi_0 - \xi_{h_0} = \frac{-2\phi_{h_0} h_0^2 t_{h_0}}{t_{n_0}^2 + \sqrt{t_{n_0}^4 + 4t_{h_0}^2 \phi_{h_0}^2 h_0^2}} \,, \tag{16}$$

where ξ_0 denotes the values of ξ_h at $h = 0$.

OCO starting at zero offset. For the zero-offset case, we need the OCO trajectory to start at the initial half-offset $h_0 = 0$ and end at the final half-offset $h \neq 0$. This reduces the set of equations (10) and (13) to

$$t^2 = t(\xi, h; \xi_0)^2 = \frac{4h^2}{V^2} + \frac{t_0(\xi_0)^2 h^2}{h^2 - (\xi - \xi_0)^2} \,, \tag{17}$$

$$\xi - \xi_0 = \frac{2\phi_0 h^2}{t_0 + \sqrt{t_0^2 + 4\phi_0^2 h^2}} \,, \tag{18}$$

where ξ_0, t_0, and ϕ_0 denote the values of ξ_{h_0}, t_{h_0}, and ϕ_{h_0} at $h_0 = 0$. Substitution of equation (18) in expression (17) yields

$$t^2 = \frac{4h^2}{V^2} + \frac{t_0}{2}\left(t_0 + \sqrt{t_0^2 + 4\phi_0^2 h^2}\right) , \tag{19}$$

which describes the OCO trajectory as a function of h.

Traveltime derivatives

There are a number of useful relationships between different types of traveltime derivatives that can be found from the set of equations (10)-(13). On the traveltime curve in the common-offset section at h, we have that $h = H(x,t)$. The derivatives of this equation with respect to ξ and h provide two important relationships between the parameters p and q and the local event slopes in the CO section, ϕ_h, and in the CMP section, ϕ_ξ, at the point (ξ, h) where these sections intersect. The fact that the total derivative of H with respect to ξ on the event is identically zero, leads to (Coimbra et al., 2012)

$$\phi_h = \left.\frac{dt}{d\xi}\right|_h = -\frac{\partial H}{\partial \xi}\left(\frac{\partial H}{\partial t}\right)^{-1} = -\frac{p}{q}, \tag{20}$$

which relates the traveltime slope ϕ in the CO section to $p = \partial H/\partial \xi$ and $q = \partial H/\partial t$. Correspondingly, from $dH/dh = 1$, we find that the traveltime slope ψ in the CMP section relates to q as

$$\psi_\xi = \left.\frac{dt}{dh}\right|_\xi = \frac{dH/dh}{\partial H/\partial t} = \frac{1}{q}. \tag{21}$$

Relationships between slopes. Hubral et al. (1996b) found another useful equation for the midpoint displacement in terms of the derivatives of H. In our notation, their equation (A29) can be written as

$$\xi_h - \xi_0 = \frac{-ph^2}{qt - h} = \frac{\phi_h h^2}{t - h\psi_\xi} , \tag{22}$$

where the second equality is a consequence of equations (20) and (21).

By equating the right side of equation (22) with the negative of the right side of equation (16), we find after some manipulations the local event slope ψ_ξ in the CMP section at ξ as a function of the local event slope ϕ_h in the CO section at h,

$$\psi_\xi = \frac{2ht(4 - \phi_h^2 V^2)}{V^2 t^2 + 4h^2 + \sqrt{16h^4 - 4h^2 t^2 V^2(\phi_h^2 V^2 + 2) + t^4 V^4}} . \tag{23}$$

It is instructive to observe that for a horizontal event, i.e., in the case of $\phi_h = 0$, equation (23) simplifies consiberably to

$$\psi_\xi = \frac{4h}{V^2 t}. \tag{24}$$

Since equation pairs (15)-(16) and (17)-(18), describe the very same OCO trajectory in opposite directions, we can also equate the midpoint dislocations of equations (16) and (18), resulting in the relationship between the event slopes in the ZO and CO sections given by

$$\phi_0 = \phi_h\left(\frac{t_0 t}{t_n^2}\right), \tag{25}$$

where $t_n = \sqrt{t^2 - 4h^2/V^2}$ is the NMO corrected traveltime at half-offset h. Equating ϕ_0 from two different half-offsets h and h_0 allows to find the direct relationship between the event slopes at the OCO trajectory in the two CO sections at h and h_0 as

$$\phi_h = \phi_{h_0}\left(\frac{t_n^2 t_{h_0}}{t_{n_0}^2 t}\right) . \tag{26}$$

Common-shot and common-receiver slopes. Using that $\xi = (s+g)/2$ and $h = (g-s)/2$, where s and g are the source and receiver coordinates, we can also find the traveltime derivatives with respect to s and g as

$$\varphi_s = \frac{\partial t}{\partial s} = \frac{\partial t}{\partial \xi}\frac{\partial \xi}{\partial s} + \frac{\partial t}{\partial h}\frac{\partial h}{\partial s} = \frac{1}{2}\left(\frac{\partial t}{\partial \xi} - \frac{\partial t}{\partial h}\right) = \frac{\phi - \psi}{2}\,, \tag{27}$$

$$\varphi_g = \frac{\partial t}{\partial g} = \frac{\partial t}{\partial \xi}\frac{\partial \xi}{\partial g} + \frac{\partial t}{\partial h}\frac{\partial h}{\partial g} = \frac{1}{2}\left(\frac{\partial t}{\partial \xi} + \frac{\partial t}{\partial h}\right) = \frac{\phi + \psi}{2}\,. \tag{28}$$

OCO velocity and RMS velocity

Let us now briefly discuss the relationship between the OCO and RMS velocities. For the case of $h_0 = 0$ in a homogeneous medium, differentiation of equation (23) with respect to h yields

$$\frac{\partial^2 t}{\partial h^2} = \frac{\partial \psi_\xi}{\partial h} = \frac{2t(4 - \phi_h^2 V^2)}{V^2 t^2 + 4h^2 + \sqrt{16h^4 - 4h^2 t^2 V^2(\phi_h^2 V^2 + 2) + t^4 V^4}} + \mathcal{O}(h)\,. \tag{29}$$

The second traveltime derivative in the CMP section at $h = 0$ is closely related to the NMO velocity v_n. Because v_n defines the hyperbolic traveltime approximation $t^2 = t_0^2 + 4h^2/v_n^2$, expression (29) taken at $h = 0$ and multiplied by t_0 yields

$$t_0 \left.\frac{\partial^2 t}{\partial h^2}\right|_{h=0} \equiv \frac{4}{v_n^2} = \frac{4}{V^2} - \phi_0^2\,, \tag{30}$$

or

$$\frac{4}{V^2} = \frac{4}{v_n^2} + \phi_0^2\,. \tag{31}$$

While this expression may be hard to interpret in the general case, it is instructive to note that for a stack of dipping layers with dip angle β_0, $v_n = v_{rms}/\cos\beta_0$ and $\phi_0 = 2\sin\beta_0/v_{rms}$, which yields

$$V = v_{rms}\,. \tag{32}$$

Note that this identity between the OCO velocity V and the RMS velocity v_{rms} is true at the very beginning of the OCO trajectory at zero offset. For OCO trajectories traced from another initial offset, V will deviate from the RMS velocity. In other words, OCO allows to extract offset-depending average velocities.

THE OCO STACK

The idea of the OCO stack is to construct an approximate traveltime surface using the set of equations (10), (13), and (26). The advantage of such a surface is that it uses only two traveltime attributes. These are the local event slope and the OCO velocity at the central point. Figure 2 compares a so-obtained traveltime surface to other traveltime approximations. Figure 2a shows the deviation of the OCO trajectory from the CMP traveltime. Figure 2b shows that at large offsets, the OCO trajectory leaves the CRS stacking surface. Figure 2c demonstrates that this is also true for the improved nonhyperbolic CRS stacking surface of Fomel and Kazinnik (2012). Finally, Figure 2d demonstrates the advantage of the OCO stacking surface, composed exclusively of OCO trajectories. This surface englobes the OCO trajectory of the central point at all offsets.

To construct the OCO stacking surface for a central point P_0 with coordinates (ξ_{h_0}, t_{h_0}), we trace trial OCO trajectories for each possible combination of values for V and ϕ_{h_0}. The pair that provides the maximum coherence along the trial trajectory defines the OCO trajectory for P_0. For a simple one-reflector model (see Figure 3), Figure 4 illustrates the procedure. For each point in the reference CO section for $h = 100$ m (Figure 4a), the noisy data (Figure 4a) are stacked along the OCO stacking surface. The maximum semblance (Figure 4e) along all trial surfaces determines the parameter pair of traveltime slope (Figure 4c) and OCO velocity (Figure 4d) that define the best-fitting OCO trajectory through the multi-coverage data. The result is a noise-attenuated stacked CO section (Figure 4f) corresponding to the reference section (which can, but need not exist among the acquired data).

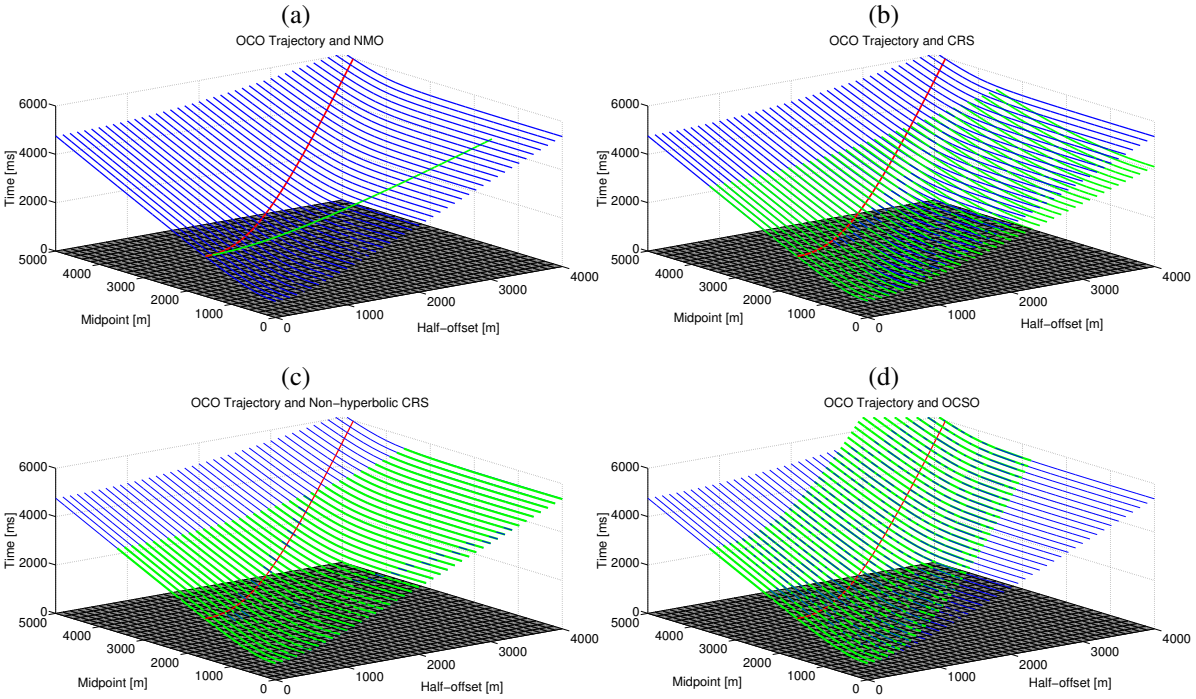

Figure 2: *Location of an OCO trajectory as compared to different traveltime curves and surfaces. (a) CMP traveltime, (b) CRS stacking surface, (c) non-hyperbolic CRS stacking surface, (d) OCO stacking surface.*

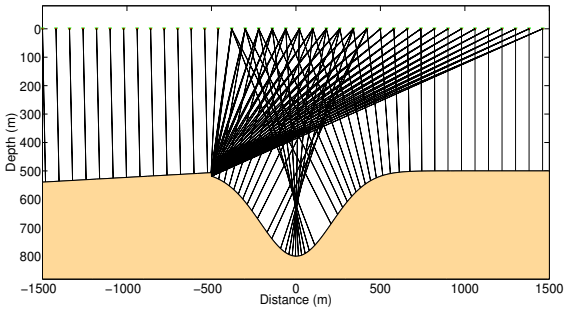

Figure 3: Model for the first synthetic test of stacking along OCO trajectories.

To incorporate information about the time dip along the trial trajectories, the coherence is evaluated along the dip direction in a small window of neighbouring traces (5 traces in our implementation) around the trajectory. At each half-offset, the dip is corrected from its initial value by means of equation (26).

To extend the so-determined OCO trajectory to an approximate traveltime surface, there are two possibilities. The most intuitive one is to join OCO trajectories for neighbouring points on the same event. This involves tracking of the event in the semblance section, which may be difficult to achieve for events with strongly varying amplitudes or noisy data. On the other hand, if handled correctly, this procedure has the potential to offer a better treatment for conflicting dips, because a single trajectory within the stacking surface, even at the central point, is of reduced importance.

Another approach is to approximate the event in the initial CO section in the vicinity of the central point P_0. In this work, we have tested the approximation by means of a Taylor expansion up to second order, which makes the method more comparable to the CRS stack. However, any other type of approximation (e.g., a Padé approximation) could also be used. Since the local event slope is already known from the

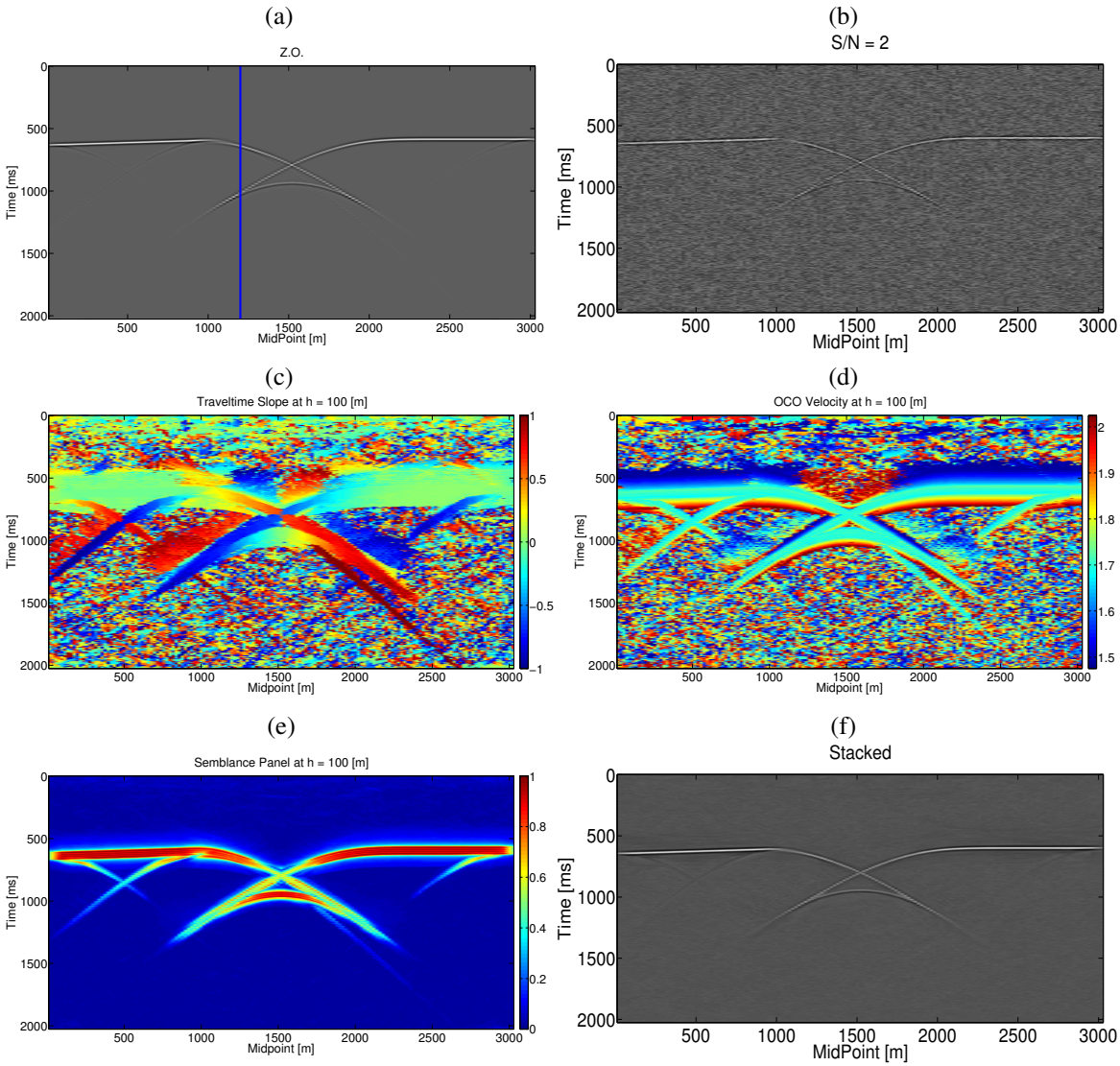

Figure 4: *(a) Reference CO section, (b) Noisy reference CO section (S/N=2), (c) Traveltime slope, (d) OCO velocity panel. (e) Semblance along OCO trajectory, (f) stacked CO section.*

previous two-parameter search, the Taylor approximation involves the search for a third parameter, the event curvature in the CO section.

The second-order Taylor approximation of the CO traveltime in the vicinity of P_0 reads

$$T(\Delta\xi_{h_0}; P_0) = \sqrt{(t_{h_0} + \phi_{h_0}\Delta\xi_{h_0})^2 + t_{h_0}K_{h_0}\Delta\xi_{h_0}^2}, \tag{33}$$

where

$$K_{h_0} = \left.\frac{\partial^2 t}{\partial \xi^2}\right|_{h=h_0} \tag{34}$$

denotes a measure of the local event curvature at the central point P_0. This parameter must be found by an additional one-parameter search.

From equation (35), the OCO stacking surface can still be obtained in two manners. The first way consists of predicting the slope of the event in the vicinity of P_0 using the traveltime approximation (35) and tracing the neighbouring OCO trajectories using these approximate slope values.

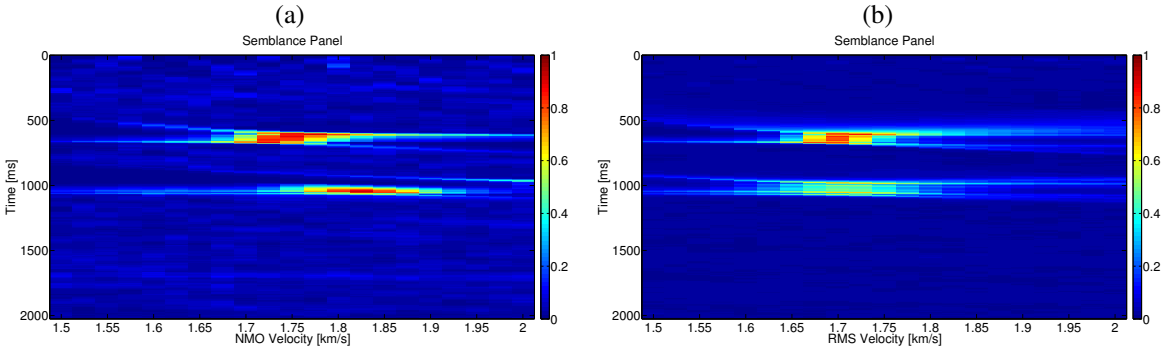

Figure 5: *Velocity spectrum for (a) conventional CMP velocity analysis, (b) OCO velocity analysis.*

The derivative of T with respect to $\Delta\xi_{h_0}$ yields the approximate slope in the vicinity of P_0 as a function of K_{h_0}, viz.

$$\Phi(\Delta\xi_{h_0}; P_0) = \frac{\partial T}{\partial \Delta\xi_{h_0}} = \frac{(t_{h_0} + \phi_{h_0}\Delta\xi_{h_0})\phi_{h_0} + t_{h_0}K_{h_0}\Delta\xi_{h_0}}{T}. \tag{35}$$

The second way consists of predicting the corresponding Taylor expansion of the event traveltime in the CO section with half-offset h from equation (35). For this purpose, the parameter K_h at h needs to be determined from K_{h_0}. The OCO stacking surface is then formed by all so-obtained Taylor expansions at all available offsets.

To transform K_{h_0} to another offset, we use the fact that on the OCO trajectory, equation (26) holds. Since this must be true for all ξ, we have

$$\frac{\partial}{\partial\xi}\left(\phi_h - \phi_{h_0}\frac{t_n^2 t_{h_0}}{t_{n_0}^2 t}\right) = 0\,, \tag{36}$$

which results in

$$K_h = K_{h_0}\frac{t_n^2 t_{h_0}}{t_{n_0}^2 t} + \phi_{h_0}\frac{\phi_h(t^2 - 4/V^2)t_{h_0}t_{n_0}^2 - \phi_{h_0}(t_{h_0}^2 - 4h_0^2/V^2)t_n^2 t}{t^2 t_{n_0}^4} \tag{37}$$

on the OCO trajectory.

Both ways of constructing the OCO stacking surface from Taylor expansion (35) yield in approximations of slightly different quality. In our tests, the procedure tracing OCO trajectories using approximate slopes was slightly superior to the one constructing approximate Taylor expansions for other offsets, particularly for large differences between h and h_0.

RESULTS AND DISCUSSION

To test the OCO stacking technique as described above, we have applied it to two synthetic data sets. The first is a multi-coverage data from a constant-velocity model and the second one is the Sigsbee2B data set.

Constant-velocity model

The first model consists of two constant-velocity layers with velocities 1.7 km/s and 1.9 km/s, separated by a reflector with two linear and a synclinal segment, including an egde that causes a diffraction event (see Figure 3). We modelled multi-coverage data using 2.5D Kirchhoff modelling and added white noise with a signal-to-noise ratio of 10. To these data, we applied the OCO stack starting at zero-offset (see Figure 4). Note that for this simple model, we stacked only along single OCO trajectories, not along OCO stacking surfaces composed of multiple trajectories. Figure 5 compares the conventional NMO velocity spectrum (no DMO correction) to the resulting OCO velocity spectrum at the CMP position indicated by a blue line in Figure 4a. At this position, there are four events with different dips in the zero-offset section (one reflection from the linear segment and two from the synclinal part, as well as the diffraction event).

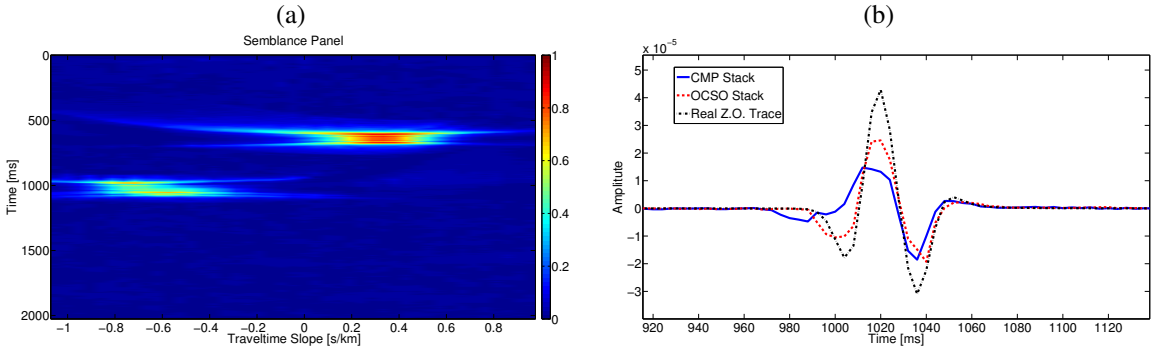

Figure 6: *(a) Dip angle as estimated from OCO stack. (b) Stacked ZO trace from OCO and CMP compared to true modelled ZO trace.*

Their different dips causes the peaks in the CMP velocity spectrum (Figure 5a) to be positioned at different velocities. We see that the OCO stack not only gets the velocity right for all four events (Figure 5b), but also provides better focused peaks that allows for a more reliable velocity extraction.

In addition to its better properties for velocity extraction, the OCO stack provides additional information on the dip of the reflection event in the stacked section (Figure 6a). It is clearly visible that the top reflector has a positive dip and the bottom reflector has a negative dip. This information cannot be extracted from the NMO velocities since any dip always shifts the NMO velocities to higher velocities by a factor of $1/\cos\theta$, where θ is the dip angle. Since such a dip spectrum can be obtained for any half-offset (independently of whether the respective section is available in the acquired data or not), slope information can be extracted for all offsets of interest. This is valuable information for slope-based methods like stereotomography (Billette and Lambaré, 1998; Billette et al., 2003) or parsimonious migration (Hua and McMechan, 2001, 2003) and migration velocity analysis (Lambaré et al., 2008).

Finally, the quality of the resulting stacked section is evaluated in Figure 6b, which shows compares the stacked ZO trace from OCO and CMP and compares them to the true modelled ZO trace at the same position. Both stacked traces are scaled by the number of traces stacked to allow for comparison. We see that the pulse recovered by the OCO stack resembles the true one much more closely than the one obtained by a CMP stack.

Sigsbee2B data

For a more realistic example, we applied the OCO stack to the Sigsbee2B data. Figure 7a shows a short-offset ($h_0 = 90$ m) section, together with the central point (blue line) where the analysis was carried out. For the analysis, we added white noise with an S/N ration of 10 to these data. The resulting velocity and dip spectra are shown in Figure 7b-d. We see that the resulting OCO velocities (Figure 7b) are slightly shifted to lower velocities in comparison to the NMO velocities (Figure 7c), accounting for the slight dips at the chosen central point. Moreover, like in the previous example, the OCO velocity peaks are again better focused than those of the NMO velocities, allowing for more reliable velocity picks. In addition to the velocity information, the OCO stack also provides information about the event slope at the central point in the stacked section (Figure 7d). The semblance maxima indicate predominantely left-dipping events in the region between 4 s and 7 s and more or less horizontal events between 7 s and 9 s two-way time.

The biparametric search that results in the two OCO panels in Figures 7b and c took 3h20min in a simple matlab implementation.

CONCLUSIONS

We have developed a new method for stacking data into zero or common-offset sections. The method uses the tracing of offset continuation (OCO) trajectories. These trajectories describe the position of a selected point on a seismic reflection event as a function of offset. Neighbouring OCO trajectories form a stacking surface along which the data can be summed up. In this way, stacked common-offset sections can be constructed for any arbitrary offset. An OCO trajectory is described by only two parameters, being an average

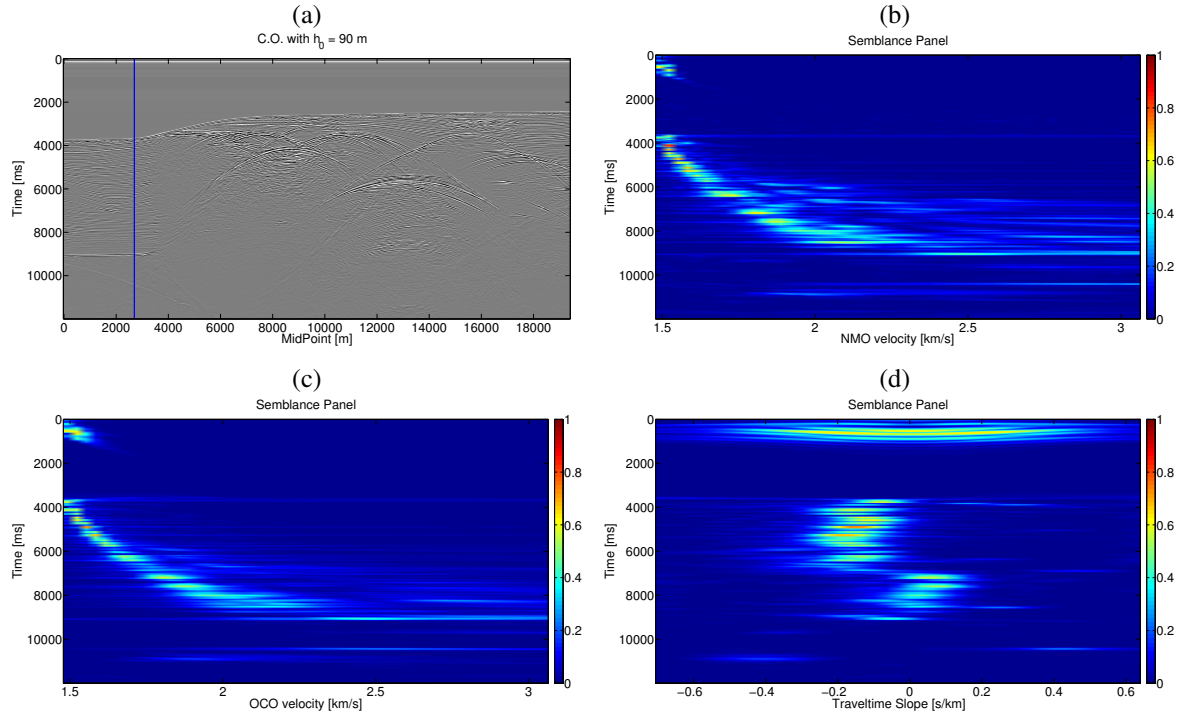

Figure 7: *Sigsbee2B data: (a) Short-offset section, (b) conventional CMP velocity spectrum, (c) OCO velocity spectrum, (d) dip angle as estimated from OCO stack.*

velocity that is an approximation to RMS velocity, and the local event slope in the final stacked section. To describe the full OCO stacking surface, one can use an additional curvature-dependent parameter to avoid event tracking in the stacked section. This procedure is still advantageous over an offset CRS stack, which needs at least 5 parameters to describe the stacking surface. Two synthetic examples for a simple constant-velocity model and the Sigsbee2B data have demonstrated that the OCO velocity spectra are more focused than conventional CMP spectra, allowing for more reliable velocity picks. Additionally, the OCO stack can provide a spectrum of local event slopes for all offsets of interest. This is valuable information for slope-based methods like stereotomography or parsimonious migration.

ACKNOWLEDGEMENTS

The authors thank SMAART-JV for providing the Sigsbee2B data and model. This work was kindly supported by the Brazilian agencies CAPES, FINEP, and CNPq, as well as Petrobras and the sponsors of the *Wave Inversion Technology (WIT) Consortium*.

REFERENCES

Bagaini, C. and Spagnolini, U. (1993). *Common-shot velocity analisys by shot continuation operators*, pages 673–676. SEG, Expanded Abstracts.

Bagaini, C. and Spagnolini, U. (1996). 2D continuation operators and their applications. *Geophysics*, 61:1846–1858.

Bagaini, C., Spagnolini, U., and Pazienza, V. (1994). *Velocity analisys and missing offset restoration by prestack continuation operators*, pages 673–676. SEG, Expanded Abstracts.

Billette, F. and Lambaré, G. (1998). Velocity macro-model estimation from seismic reflection data by stereotomography. *Geophysical Journal International*, 135(2):671–690.

Billette, F., Le Bégat, S., Podvin, P., and Lambaré, G. (2003). Practical aspects and applications of 2D stereotomography. *Geophysics*, 68(3):1008–1021.

Biondi, B., Fomel, S., and Chemingui, N. (1998). Azimuth moveout for 3-D prestack imaging. *Geophysics*, 63:574–588.

Black, J., Schleicher, K., and Zhang, L. (1993). True-amplitude imaging and dip moveout. *Geophysics*, 58(1):47–66.

Bleistein, N., Cohen, J., and Jaramillo, H. (1999). True-amplitude transformation to zero offset of data from curved reflectors. *Geophysics*, 64:112–129.

Bolondi, G., Loinger, E., and Rocca, F. (1982). Offset continuation of seismic sections. *Geophysical Prospecting*, 30:813–828.

Bolondi, G., Loinger, E., and Rocca, F. (1984). Offset continuation in theory and pratice. *Geophysical Prospecting*, 32:1045–1073.

Canning, A. and Gardner, G. H. F. (1996). Regularizing 3D data sets with DMO. *Geophysics*, 61:1101–1114.

Chemingui, N. and Biondi, B. (2002). Seismic data recostruction by inversion to common offset. *Geophysics*, 67:1575–1585.

Coimbra, T. A., Novais, A., and Schleicher, J. (2012). Offset continuation (OCO) ray tracing using OCO trajectories. *Stud. Geophys. Geod.*, 56:65–82.

Collins, C. L. (1997). Imaging in 3D DMO; Part I: Geometrical optics model; Part II: Amplitude effects. *Geophysics*, 62:211–244.

Courant, R. and Hilbert, D. (1989). *Methods of Mathematical Physics*, volume II. Wiley-Interscience.

Deregowski, S. M. and Rocca, F. (1981). Geometrical optics and wave theory of constant offset sections in layered media. *Geophysical Prospecting*, 29:374–406.

Fomel, S. (1994). Kinematically equivalent differential operator for offset continuation of reflected wave seismograms. *Russian Geology and Geophysics*, 35(9):122–134.

Fomel, S. (2003). Theory of differential offset continuation. *Geophysics*, 68:718–732.

Fomel, S. and Kazinnik, R. (2012). Non-hyperbolic common reflection surface. *Geophysical prospecting*, 60:1–7.

Gelchinsky, B., Berkovitch, A., and Keydar, S. (1999). Multifocusing homeomorphic imaging - Part 1. Basic concepts and formulas. *Journal of Applied Geophysics*, 75:229–242.

Hale, I. D. (1984). Dip-moveout by fourier transform. *Geophysics*, 49:741–757.

Hertweck, T., Schleicher, J., and Mann, J. (2007). Data stacking beyond CMP. *The Leading Edge*, 26(7):818–827.

Hua, B. and McMechan, G. A. (2001). Parsimonious 2-D poststack Kirchhoff depth migration. *Geophysics*, 66(5):1497–1503.

Hua, B. and McMechan, G. A. (2003). Parsimonious 2D prestack Kirchhoff depth migration. *Geophysics*, 68(3):1043–1051.

Hubral, P., Schleicher, J., and Tygel, M. (1996a). A unified approach to 3-D seismic reflection imaging - Part I:Basic concepts. *Geophysics*, 61:742–758.

Hubral, P., Tygel, M., and Schleicher, J. (1996b). Seismic image waves. *Geoph. J. Int.*, 125:431–442.

Jäger, R., Mann, J., Hocht, G., and Hubral, P. (2001). Common-reflection-surface stack: Image and attibutes. *Geophysics*, 66:97–109.

Lambaré, G., Touré, J.-P., Moigne, J. L., Zimine, S., Herrmann, P., Carbonara, S., and Federici, F. (2008). Velocity update for pre-stack time migration. In *Annual International Meeting, SEG, Expanded Abstracts*, pages 3250–3254.

Perroud, H. and Tygel, M. (2004). Nonstretch NMO. *Geophysics*, 69:599–607.

Salvador, L. and Savelli, S. (1982). Offset continuation for seismic stacking. *Geophysical Prospecting*, 30:829–849.

Santos, L., Scheicher, J., and Tygel, M. (1997). 2.5-D true-amplitute offset continuation. *J. Seism. Expl.*, 6:103–116.

Schleicher, J. and Bagaini, C. (2004). Controlling amplitudes in 2.5D commom-shot migration to zero offset. *Geophysics*, 69:1299–1310.

Silva, E. (2005). *Horizon velocity analisys using OCO rays*, pages 372:1–4. SBGf, 9o Congresso Internacional de Geofísica.

Stolt, R. (2002). Seismic data mapping and reconstruction. *Geophysics*, 67:890–908.

Tygel, M., Scheicher, J., Hubral, P., and Santos, L. (1998). 2.5-D true-amplitute Kirchhoff migration to zero offset in laterally inhomogeneous media. *Geophysics*, 63:557–573.

Tygel, M., Schleicher, J., and Hubral, P. (1996). A unified approach to 3-D seismic reflection imaging - Part II:Theory. *Geophysics*, 61:759–775.

Zhang, Y., Bergler, S., and Hubral, P. (2001). Common-reflection-surface (CRS) stack for common offset. *Geophysical Prospecting*, 49:709–718.